

DETECTION OF FLOODS IN SAR IMAGES WITH NON-LINEAR KERNEL CLUSTERING AND TOPOGRAPHIC PRIOR

F. de Morsier, M. Rasamimalala, D. Tuia[‡], M. Borgeaud[°], S. Rakotoniaina*, S. Rakotondraompiana* and J.-Ph. Thiran*

LTS 5, École Polytechnique Fédérale de Lausanne, Switzerland

*Institute and Observatory of Geophysics Antananarivo (IOGA), University of Antananarivo, Madagascar

[‡]LaSIG, École Polytechnique Fédérale de Lausanne, Switzerland

[°] European Space Agency, ESRIN, Frascati, Italy

ABSTRACT

After a major flood catastrophe, a precious information is the delineation of the affected areas. Remote sensing imagery, especially synthetic aperture radar, allows to obtain a global and complete view of the situation. However, the detection of the flooded areas remains a challenge, especially since the reaction time for ground teams is very short. This makes the application of automatic detection routines appealing. Such methods must avoid complex parametrization, heavy computational time and long intervention by the operator. We propose an automatic three steps strategy, starting by re-balancing the different types of pixels (non-water, permanent water and flooded) using digital elevation model information, then isolating water pixels and finally separating flooded from permanent water pixels using non-linear clustering in dedicated feature spaces. Experiments on two sets of ASAR images show the effectiveness of the method competing with supervised standard log-ratio thresholding.

Index Terms— log-ratio, feature space, Synthetic Aperture Radar, change detection, remote sensing, kernel methods

1. INTRODUCTION

When a major catastrophe strikes, one of the most impelling needs is the allocation of human resources on the field. In recent years, Earth observation has shown its potential to provide a global image of affected regions and has been acknowledged to play a major role in the allocation of human resources. In the case of floods, that often happen in conjunction with heavy rains and cloud cover, the recourse to Synthetic Aperture Radar (SAR) becomes almost compulsory [1]: SAR imagery is not affected by weather conditions and, since it does not rely on sunlight, can also be operated at night. For this reasons, there has been a strong research current dealing with the development of change (flood) detection tools using this type of imagery. Among the many techniques deployed in the literature, techniques based on the log-ratio image have shown desirable properties and are

enabled by an easy access to reference non-flooded SAR images. After transformation of the data, the methods rely on automatic thresholding, modelling the distributions either using generalized Gaussians [2], Nakagami-Gamma, Weibull or log-normal [3] models. The unsupervised estimation of distribution parameters can be done through Expectation-Maximization algorithms [4].

In flood detection problems, the flood class is often weakly represented and is therefore unseen in an histogram of the backscattering values. Thresholding methods fitting a certain distribution on the histogram fail at detecting the small flood class present in the lower backscattering values of the flooded image. For this reason, the change detection approaches require a way of focusing automatically on water pixels in order to be used for flood detection. In [5], an approach based on multiple tiles is proposed to detect thresholds per tile to be more robust to this small sample problem. In [6], flood detection is performed on a single post-event image by segmenting the flooded region in a semi-automatic fashion with an active contour model in conjunction with the rivers' network. The final distinction between permanent water and flooded regions is taken by supervised classification. In [7], a robust segmentation of very high resolution SAR images uses morphological profiles at multiple scales to remove speckle noise. The final classification exploits an electromagnetic model simulating the backscattering of the landcover types.

Digital Elevation Models (DEM) can be used to overcome the small sample problem and improve the flood detection robustness. The probability of floods is higher in low altitude regions, low-slope regions and concave areas, as well as in regions close to water bodies (rivers, lakes). This information can be integrated in a model, for example in a fuzzy classification scheme [8].

In this paper, we propose to use a non-parametric unsupervised approach with landscape topography as flooding prior, followed by non-linear clustering in an appropriate Reproducible Kernel Hilbert Spaces (RKHS) to detect flooded areas.

2. METHODOLOGY

Consider two registered SAR backscattering images X^{t_1} and X^{t_2} acquired at two times steps t_1 and t_2 . To derive the flood-induced changes between the acquisitions, different combinations of the images can be used. The widely used log-ratio, $LR = \log\left(\frac{X^{t_1}+a}{X^{t_2}+a}\right) = \log(X^{t_1}+a) - \log(X^{t_2}+a) = X_{log}^{t_1} - X_{log}^{t_2}$, with $a = 0.1$ to avoid infinite values, has an histogram characterized by three modes: a major mode ($LR \approx 0$) for the unchanged pixels, a positive mode ($LR \gg 0$) for pixels showing an increase of backscattering and a negative mode ($LR \ll 0$) for pixels showing a decrease of backscattering. The latter mode corresponds to flooded pixels, which show low backscattering values at time t_2 . These different modes are extremely unbalanced, typically with a very small number of pixels corresponding to flooded areas, when compared to the unchanged (permanent water and non-water) pixels. Thus, it is very difficult to fit a specific distribution to this last mode without using prior knowledge. The proposed methodology is a three steps strategy (see Fig. 1):

- STEP 1: Balance the classes of non-water, permanent water and flooded by importance sampling (IS) based on a “flooding” probability derived from DEM features (*a priori* information).
- STEP 2: Isolate water pixels at t_2 using clustering on the backscattering values of $X_{log}^{t_2}$.
- STEP 3: Separate flooded from permanent water pixels using non-linear clustering on the log-ratio or ratio between the two images.

The 2D plot in Fig. 1 represents the pixels along the log-ratio and the log-scaled image $X_{log}^{t_2}$, respectively, as well as the three steps described in the next sections.

2.1. Importance sampling from “flooding” probability

In flood detection problems, the pixels of interest often represent a very small percentage of the image. Moreover, in images covering large regions, it cannot be assumed that flooded regions will represent a large fraction. In order to overcome this small sample problem, we propose to sub-sample the image according to some *a priori* knowledge on how a flood is likely to happen in the different regions of the image. Floods are more likely to happen along river networks and in regions having specific geomorphological attributes. Flat and concave regions have higher probability of being flooded [8]. We propose a flooding probability function based on terrain altitude, slope and concavity, derived from a DEM and on the proximity to water bodies.

Let us consider the altitude Z . The terrain slope is obtained as the norm of the smoothed (\check{Z}) horizontal and vertical gradient: $|\nabla(Z)| = \sqrt{\nabla_h(\check{Z})^2 + \nabla_v(\check{Z})^2}$ which shows

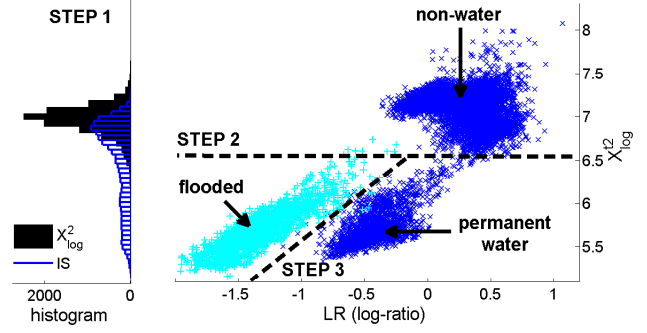


Fig. 1. 2D plot of the log-ratio and log-scaled flooded image at time t_2 . A clustered structure can be observed between flooded, permanent water and non-water pixels. The left histogram shows the typical unbalanced situation between abundant non-water and water pixels (plain black) and after importance sampling (IS) at STEP 1 (blue stripes), which rebalances the histogram using flooding probability. STEP 2 isolates water pixels and STEP 3 detects the flooded pixels.

low values in flat regions. The concavity is obtained from the difference of two Gaussians convoluted with the Z (DoG), as in [9]. The second Gaussian bandwidth, the subtracted one, is chosen smaller than the first one to have the highest DoG values corresponding with most concave regions. The smoothed negative $\check{X}_{log}^{t_2}$ indicates water proximity. These terms are combined into a “flooding” probability with the following expression:

$$p(\text{flooding}|Z, |\nabla(Z)|, DoG(Z)) = \frac{1}{4} [\tau(-Z) + \tau(-|\nabla(Z)|) + \tau(DoG(Z)) + \tau(-(\check{X}_{log}^{t_2}))] \quad (1)$$

with $\tau(\cdot)$ a normalization operator clamping each term between 0 and 1. Each factor is equally weighted since they are all taken as pseudo probability with equal prior. The prior weights could be learned in a supervised setting. Here equal prior is sufficient as initialization before performing our clustering. The flooding probability from Eq. (1) is high in low altitude, flat and concave regions close to water bodies. A Gaussian distribution is fitted to $p(\text{flooding}|\dots)$ with mean μ_f and standard deviation σ_f . Our IS scheme takes the N_f most probable pixels having $p(\text{flooding}|\dots) > \mu_f + 2\sigma_f$. In Fig. 2, examples of the different attributes and the corresponding flooding probability are presented.

2.2. Isolating water areas in post-event image

The distinction of water and non-water pixels in the image $X_{log}^{t_2}$ (see Fig. 1 STEP 2) is performed with a clustering approach. This strategy allows to perform detection in a com-

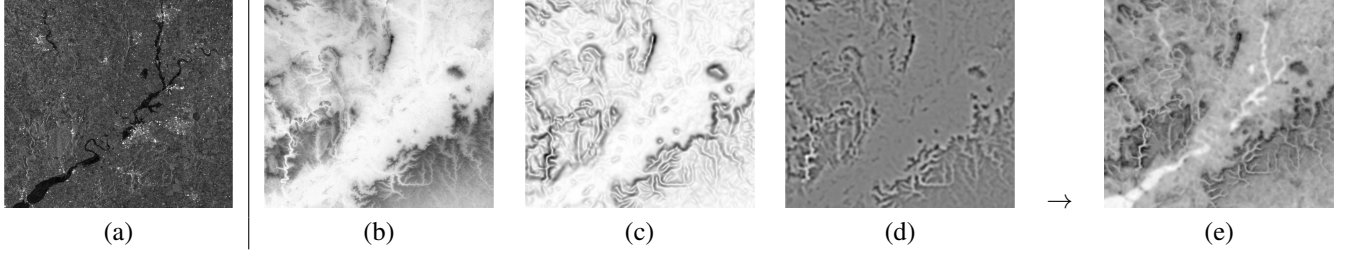


Fig. 2. (a) SAR backscattering over *Tewkesbury* region after floods, (b) negative DEM altitude, (c) negative gradient norm, (d) concavity and (e) resulting flooding probability.

pletely unsupervised way, since it does not require user intervention to initialize the flooded region, contrarily to active contour methods [6]. The IS step (STEP 1) described previously facilitates the task of separating the two clusters, since the histogram to be partitioned is less biased towards non-water pixels. Nonetheless, a bias can still remain towards non-water pixels and fitting a mixture of 2 Gaussians or partitioning using linear k -means algorithm would still fail at separating the two groups correctly. For these reasons, we opted for a nonlinear clustering methods, kernel k -means, which has already shown desirable properties in unsupervised change detection [10].

The kernel k -means partitioning algorithm minimizes the sum-of-square distances among the cluster center and the samples attributed to the center in a feature space induced by a mapping function Φ [11]. This mapping function Φ enables the algorithm to handle non-Gaussian clusters of different sizes. Given samples $x_i \in X, i = 1, \dots, N$ and K cluster centers, the within-group scattering to be minimized is

$$S_w = \frac{1}{N} \sum_{k=1}^K \sum_{i \in C_k} \|\Phi(x_i) - \mu_k\|^2 \quad (2)$$

with C_k the set of samples corresponding to cluster k and μ_k its center. The center can be expressed as $\mu_k = \frac{1}{N_k} \sum_{i \in C_k} \Phi(x_i)$. By replacing the center expression in Eq. (2), the within-group scattering can be expressed in terms of dot products among the mapped samples $\Phi(x_i)$ and kernel functions $k(x, x) = \langle \phi(x), \phi(x) \rangle$ can be applied. By doing so, Eq. (2), scaled by N , becomes

$$N \cdot S_w = k(x_i, x_i) - \frac{2}{N_k} \sum_{j \in Z_k} k(x_i, x_j) + \frac{1}{N_k^2} \sum_{j, l \in Z_k} k(x_j, x_l) \quad (3)$$

2.3. Flood detection with composite kernels

Once the water pixels have been isolated, it is possible to distinguish permanent water from flooded areas (STEP 3). This is usually done by thresholding the log-ratio [2, 3]. However, the optimal separation is not a vertical threshold on the log-ratio as depicted in Fig. 1 but function of the backscattering values of X_{log}^{t2} (diagonal separation in the figure).

To this purpose, it is common to use the ratio image: $X = \frac{X^{t1}}{X^{t2} + \epsilon}$, ϵ being added to avoid singularities, or the log-ratio image: $X = X_{log}^{t1} - X_{log}^{t2}$ and then to map these inputs in an appropriate Reproducing Kernel Hilbert space (RKHS) space using a kernel function (see Section 2.2). In the experiments, we will refer to this strategies as ‘*Input Space*’, since the ratios are computed directly using the original images. To be more specific to the change detection problem, we also extended this straightforward formulation to more complex feature spaces, where the ratio images are computed directly in the RKHS feature space [12] to provide more flexibility in fitting the data. In the experiments, we will refer to these strategies as ‘*Feature space*’.

The image ratio in the feature space can be defined as $\Phi(\cdot)_{ratio} = \frac{\{(\sqrt{\gamma} \mathbf{A}^2 \varphi(X^{t2}))^T, (\mathbf{A}^1 \varphi(X^{t1}))^T\}^T}{\sqrt{\langle \mathbf{A}^2 \varphi(X^{t2}), \mathbf{A}^2 \varphi(X^{t2}) \rangle}}$, with \mathbf{A}^t a symmetric positive definite scaling matrix and $\varphi(\cdot)$ the implicit mappings. Following this idea, the kernel is expressed as

$$K_{\Phi_{ratio}}(x_i, x_j) = \frac{K(x_i^{t1}, x_j^{t1})}{K(x_i^{t2}, x_j^{t2}) + \epsilon} + \gamma \delta_{ij} \quad (4)$$

The regularization parameter $\gamma = 10^{-8}$ is added to kernel’s diagonal to ensure its positive definiteness.

The log-ratio image can be defined similarly to the difference image in the feature space in [12] using the log of the images, since this is equivalent to the logarithm of the ratio. The difference of the log images in the feature space is $\Phi(\cdot)_{log-ratio} = \mathbf{A}^2 \varphi(X_{log}^{t2}) - \mathbf{A}^1 \varphi(X_{log}^{t1})$. The associated kernel is expressed as

$$K_{\Phi_{log-ratio}}(x_i, x_j) = K(x_{log,i}^{t1}, x_{log,j}^{t1}) + K(x_{log,i}^{t2}, x_{log,j}^{t2}) - K(x_{log,i}^{t1}, x_{log,j}^{t2}) - K(x_{log,i}^{t2}, x_{log,j}^{t1}) \quad (5)$$

This composition of kernels exhibits the two single time kernels (for X^{t1} and X^{t2}) and the cross-time kernels encoding similarities between images at time t_1 and t_2 .

2.4. Post-processing

The spatial location of detected flooded pixels should be exploited to reduce false alarms. Since flooded regions are not extremely localized but grouped over connected locations, isolated pixels detected as flooded have high chances of being false alarms. To reduce their number, a median filter with a window of 5×5 pixels is convoluted with the output of our flood detection algorithm.

3. EXPERIMENTS

3.1. Data & preprocessing

To test the proposed methodology, we considered two challenging SAR datasets. Both are composed of two ENVISAT-ASAR multilook images (150m resolution) and a DEM (30m resolution) from ASTER:

- *Kinkony*: Two SAR images acquired respectively on October 19th, 2011 during dry season and on February 16th, 2012 just after a cyclone strike in the North of Madagascar. See top row of Fig. 3.
- *Tewkesbury*: Two SAR images acquired on May 30th and on July 23rd 2007, respectively before and after an important flood event in Gloucestershire, U.K. See bottom row of Fig. 3.

The images and the DEM are co-registered using georeferenced tie points. A 3×3 Enhanced Lee filter is used to reduce the speckle noise in the SAR images. The number of pixels after sub-sampling (importance or random sampling) is set to $N = 1000$. The test set consist in 8351 and 7116 pixels respectively. The DoG standard deviations are set experimentally to 8 and 6. The gradient of the altitude Z is smoothed by a Gaussian $\mathcal{N}(0, 6)$. The kernels are radial basis function (RBF) with a bandwidth parameter set to the sum of the standard deviation of the different variables. For stability reasons, bandwidths of the dedicated kernels in a composition are set equal to each other.

Results for both experiments are reported in terms of Cohen's κ statistic in Table 1, along with the Support Vector Data Description (SVDD) using an RBF kernel trained with 100 flooded pixels, and the standard supervised log-ratio threshold maximizing the κ accuracy using a training set of 1000 labeled pixels (500 flooded and 500 non-flooded). Note that the comparative approaches are thus eased by the presence of labeled pixels, while our proposed method is completely unsupervised.

3.2. Results and discussion

The IS at STEP 1 is affecting drastically the results of both datasets, with the exception of the case considering the log-ratio in the feature space in STEP 3: in that case better results

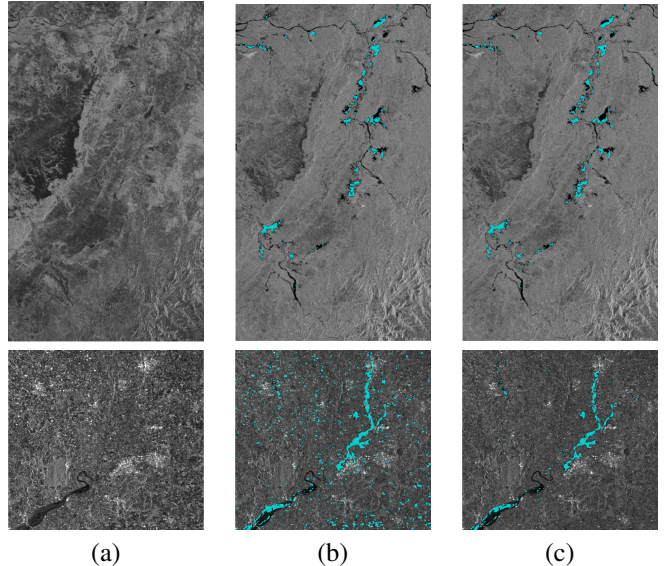


Fig. 3. (a) SAR images before the floods. (b) Flood detection result (in light blue) using supervised log-ratio thresholding; (c) Detection using the proposed method using the ratio in Feature Space (Kinkony, top row) or the log-ratio in Input space (Tewkesbury, bottom). All the detection maps are post-processed and overlaid on the SAR image after flooding.

are obtained with random sampling. The ratio in the feature space gives the best κ accuracy with importance sampling. In *Tewkesbury*, IS strongly affects the results and leads to better results for the ratio and log-ratio in input space only. The variability and low results for the in 'Feature space' experiments are due to a series of non-water pixels clustered as water in STEP 2. These outliers result in biased separation of flooded and permanent water clusters at STEP 3. These remaining pixels of non-water can induce a radically different separation for the more complex feature mappings (ratio and log-ratio in feature space), sometimes pushing the boundary almost orthogonally to the ideal separation depicted in Fig. 1. Our unsupervised approach compared to the supervised log-ratio thresholding reaches equivalent or better results for both datasets. Moreover, the flood detection maps are neater with less false alarms (see the two right columns of Fig. 3).

4. CONCLUSION

We proposed a three-steps strategy for unsupervised flood detection. First, the distribution of water pixels is enhanced by importance sampling based on a prior on topography and then water areas are detected with nonlinear clustering. Finally, the flooded pixels are distinguished from permanent waters using non-linear clustering on the ratio or log-ratio images in dedicated feature spaces through appropriate composite kernels. The experiments show the benefit of importance sampling prior to clustering and similar accuracies than super-

Dataset Ratios in Ratio type		<i>Kinkony</i>				<i>Tewkesbury</i>			
		Input space		Feature space		Input space		Feature space	
		ratio	log-ratio	ratio	log-ratio	ratio	log-ratio	ratio	log-ratio
RS	Raw	0.48 (0.26)	0.32 (0.38)	0.26 (0.40)	0.86 (0.08)	0.48 (0.01)	0.48 (0.02)	0.34 (0.16)	0.41 (0.05)
	PP	0.48 (0.25)	0.32 (0.38)	0.25 (0.40)	0.93 (0.06)	0.53 (0.01)	0.53 (0.02)	0.36 (0.19)	0.51 (0.07)
IS	Raw	0.96 (0.01)	0.93 (0.02)	0.98 (0.01)	0.39 (0.41)	0.64 (0.00)	0.67 (0.00)	0.45 (0.03)	0.32 (0.03)
	PP	0.97 (0.01)	0.95 (0.02)	0.99 (0.01)	0.38 (0.42)	0.68 (0.00)	0.72 (0.00)	0.47 (0.03)	0.32 (0.03)
LR Raw		0.97 (0.01)				0.64 (0.01)			
LR PP		0.98 (0.00)				0.71 (0.00)			
SVDD Raw		0.97 (0.00)				0.63 (0.00)			
SVDD PP		0.98 (0.00)				0.70 (0.00)			

Table 1. Averaged κ over 10 random runs. RS: Random Sampling, IS: Importance Sampling, LR: log-ratio thresholding (supervised), PP: post-processed (Section 2.4), SVDD trained with 100 samples.

vised log-ratio thresholding. Future research will consider the robustness of the two first steps for the definition of the complex feature spaces, the use of other clustering algorithms and the extension to very-high resolution SAR images.

5. ACKNOWLEDGMENTS

This work has been partially funded by the Swiss National Science Foundation (grant PZ00P2-136827), by the EPFL CODEV (SEED MONEY) and by RUAG Schweiz AG (C. Küchler). The authors also would like to acknowledge Philippe Bally (ESA) for granting us the access to SAR data.

6. REFERENCES

- [1] S.B. Serpico, S. Dellepiane, G. Boni, G. Moser, E. Angiati, and R. Rudari, “Information extraction from remote sensing images for flood monitoring and damage evaluation,” *Proc. of the IEEE*, vol. 101, no. 3, pp. 631–651, 2012.
- [2] Y. Bazi, L. Bruzzone, and F. Melgani, “An unsupervised approach based on the generalized Gaussian model to automatic change detection in multitemporal SAR images,” *IEEE Trans. Geosci. Remote Sens.*, vol. 43, no. 4, pp. 874–887, 2005.
- [3] G. Moser and S.B. Serpico, “Generalized minimum-error thresholding for unsupervised change detection from SAR amplitude imagery,” *IEEE Trans. Geosci. Remote Sens.*, vol. 44, no. 10, pp. 2972–2982, 2006.
- [4] G. Moser and S.B. Serpico, “Unsupervised change detection from multichannel SAR data by Markovian data fusion,” *IEEE Trans. Geosci. Remote Sens.*, vol. 47, no. 7, pp. 2114–2128, 2009.
- [5] S. Martinis, A. Twele, and S. Voigt, “Unsupervised extraction of flood-induced backscatter changes in SAR data using Markov image modeling on irregular graphs,” *IEEE Trans. Geosci. Remote Sens.*, vol. 49, no. 1, pp. 251–263, 2011.
- [6] D.C. Mason, R. Speck, B. Devereux, G.J.P. Schumann, J.C. Neal, and P.D. Bates, “Flood detection in urban areas using TerraSAR-X,” *IEEE Trans. Geosci. Remote Sens.*, vol. 48, no. 2, pp. 882–894, 2010.
- [7] L. Pulvirenti, M. Chini, N. Pierdicca, L. Guerriero, and P. Ferrazzoli, “Flood monitoring using multi-temporal COSMO-SkyMed data: Image segmentation and signature interpretation,” *Remote Sens. Environ.*, vol. 115, no. 4, pp. 990–1002, 2011.
- [8] N. Pierdicca, M. Chini, L. Pulvirenti, and F. Macina, “Integrating physical and topographic information into a fuzzy scheme to map flooded area by SAR,” *Sensors*, vol. 8, no. 7, pp. 4151–4164, 2008.
- [9] L. Foresti, D. Tuia, M. Kanevski, and A. Pozdnoukhov, “Learning wind fields with multiple kernels,” *Stoch. Env. Res. Risk. Ass.*, vol. 25, no. 1, pp. 51–66, 2011.
- [10] M. Volpi, D. Tuia, G. Camps-Valls, and M. Kanevski, “Unsupervised change detection with kernels,” *IEEE Geosci. Remote Sens. Lett.*, vol. 9, no. 6, pp. 1026–1030, 2012.
- [11] M. Girolami, “Mercer kernel-based clustering in feature space,” *IEEE Trans. Neural Netw.*, vol. 13, no. 3, pp. 780–784, 2002.
- [12] G. Camps-Valls, L. Gómez-Chova, J. Muñoz-Marí, J. Luis Rojo-Álvarez, and M. Martínez-Ramón, “Kernel-based framework for multi-temporal and multi-source remote sensing data classification and change detection,” *IEEE Trans. Geosci. Remote Sens.*, vol. 46, no. 6, pp. 1822–1835, 2008.